Journal of the European Ceramic Society 7 (1991) 209–218

Duplex Ceramics: I. Stress Calculations, Fabrication and Microstructure

H. E. Lutz* & N. Claussen

Technical University of Hamburg-Harburg, Advanced Ceramics Group, W-2100 Hamburg 90, Germany

(Received 10 July 1990; accepted 7 November 1990)

Abstract

The microstructural design concept of duplex ceramics is based on relatively large (10–50 μm) spherical zones dispersed in a ceramic matrix. The zones contain variable fractions of ZrO_2 particles. On cooling from the fabrication temperature they expand relative to the matrix either completely during cooling or at first partially and then continue by stress induction. Compressive stresses are developing within and radially around the zones. Tensile hoop stresses are created tangentially around the zones. A stress calculation is presented for the prediction of crack initiation and propagation processes at radial defects at the zone–matrix interface. The predictions are compared with observations. It is found that the sintering behaviour of the components and the fabrication conditions are of great importance for the performance of duplex structures. They influence the transformability of ZrO_2 within the zones and, hence, their effectiveness. The concept is evaluated with Al_2O_3, 2Y-TZP, 3Y-TZP, and Al_2O_3-alloyed 3Y-TZP as matrix. Monoclinic (m-) ZrO_2 and various m-ZrO_2-containing Al_2O_3 mixtures have been used as pressure zone materials.

Das Duplex-Konzept basiert auf der Einlagerung relativ großer (10–50 μm) kugeliger Zonen in eine keramische Matrix. Die Zonen enthalten unterschiedliche Anteile an ZrO_2. Beim Abkühlen von der Herstellungstemperatur dehnen sie sich relativ zur Matrix aus. Die Umwandlung vollzieht sich entweder bereits vollständig beim Abkühlen oder erst teilweise und dann vollständig durch Spannungsinduktion. Die Zonen geraten unter hydostatischen Druck, während sich um die Zonen tangentiale Zug- und radiale Druckspannungen aufbauen. Die Berechnung der Spannungsverteilung ermöglicht eine recht gute Vorhersage der spontanen Einleitung und Ausbreitung von Rissen an Zone–Matrix-Grenzflächen. Das Sinterverhalten der Matrix- und Zonenkomponenten und die Herstellungsbedingungen sind für die erfolgreiche Herstellung von Duplex-Keramiken von großer Bedeutung. Sie beeinflussen die Umwandlungsfähigkeit der ZrO_2-Teilchen in den Zonen und damit ihre Wirksamkeit. Als Matrixkomponente wurde Al_2O_3, 2Y-TZP, 3Y-TZP und Al_2O_3-legiertes 3Y-TZP verwendet. Monoklines (m-) ZrO_2 und verschiedene Mischungen aus m-ZrO_2 und Al_2O_3 dienten als Einlagerungskomponente.

Le principe d'élaboration microstructurale des céramiques duplex est basé sur la dispersion de zones sphériques relativement larges (10–50 μm) dans une matrice céramique. Ces zones contiennent des fractions variables de particules de ZrO_2. Lors du refroidissement à partir de la température d'élaboration, elles se dilatent par rapport à la matrice, soit complètement au cours du refroidissement, soit d'abord partiellement puis ensuite par induction de contraintes. Des contraintes compressives se développent à l'intérieur des zones et radialement à celles-ci. Des contraintes circulaires de tension sont crées tangentiellement à ces zones. On présente un calcul de contraintes destiné à la prévision de l'initiation des fissures et des mécanismes de propagation aux défauts radiaux de l'interface zone–matrice. Les prévisions sont comparées avec les observations effectuées. On a mis en évidence que le comportement en frittage des constituants et les conditions d'élaboration sont des paramètres déterminants pour les performances des structures duplex. Ils influencent la transformabilité de ZrO_2 à l'intérieur des zones et par conséquent, leur efficacité.

* Present address: University of Sydney, Department of Mechanical Engineering, New South Wales 2006, Australia.

Journal of the European Ceramic Society 0955-2219/91/$3.50

On a étudié ce concept avec des matrices de Al_2O_3, 2Y-TZP, 3Y-TZP et de 3Y-TZP alliée à Al_2O_3. Les matériaux utilisés pour la zone de pression étaient la ZrO_2 monoclinique (m-) et divers mélanges de Al_2O_3 contenant de la m-ZrO_2.

1 Introduction

Strength and toughness of various engineering oxide ceramics have been considerably enhanced in recent years by applying different toughening concepts.[1-4] However, in most cases, the enhanced toughness leads only to a minor increase in the critical temperature difference (ΔT_c) during thermal shock. This can be explained by the usually high thermal coefficient of expansion (α) and the temperature sensitivity of the toughness. Once ΔT_c is surpassed, the retained strength (σ_R) is usually close to zero, which is a direct consequence of the high strength, i.e. the large stored elastic energy.[5]

On the other hand, it has long been known that low strength refractories exhibit low strength degradation on severe thermal shocking. Unfortunately, most low-expansion thermal-shock resistant oxides, quartz glass, cordierite, Al_2TiO_5, etc., show low inherent strengths which usually cannot be sufficiently improved for any load-bearing engineering application. Thus, the dilemma with most oxides seems to be to engineer microstructures that exhibit either high strength or high thermal-shock resistance, but not both simultaneously.

An interesting feature of most thermal-shock damage resistant ceramics is that they exhibit a pronounced *R*-curve behavior.[6] This correlation between thermal-shock damage resistance and *R*-curve behavior was demonstrated by Swain[7] with differently treated Mg-PSZ ceramics. The conventionally aged PSZ exhibit high strength and toughness, but an intermediate thermal-shock resistance. During subeutectoid heat treatment a continuous m-ZrO_2 phase develops at the grain boundaries. The material exhibits far better thermal-shock strength degradation at slightly lower strength, but still considerable toughness. The essential difference between the two materials lies in the way the *R*-curves rise with propagating crack. For good thermal-shock resistance the long-range rising *R*-curve of the heat-treated material is more ideally suited than the short-range rising *R*-curve of the conventionally aged PSZ.

In earlier work Claussen and coworkers[8,9] introduced a microstructural design concept which is based on relatively large spherical compressive zones dispersed in a ceramic matrix. The intent of this complex microstructure is to retain the high matrix strength with the ability for crack deflection and branching, i.e. increasing crack growth resistance.[10] This would appear to offer good possibilities for the development of mechanical and thermal-shock resistant materials. However, it is well known that the presence of inclusions in glass and ceramics weakens the structure by residual stress fields around the inclusions due to thermal expansion and elastic modulus mismatch.[11-13] From fracture studies in structural ceramic materials it has been shown that fracture frequently originates from such inclusions.

The aim of this study is to improve the crack growth resistance of Al_2O_3 and ZrO_2 ceramics at high retained strength by dispersing pressure zones in these materials. It is expected that toughening in duplex ceramics can be achieved by activating mechanisms which are triggered by the interaction of a crack-tip stress field with the residual stress fields around the pressure zones. For the design of these materials it is however important that the elastic energy which is stored within and around the pressure zones does not exceed the energy which is required for crack propagation, because then no toughening would be achieved. The stimulation of inelastic deformation by crack deflection and crack-branching processes is expected to produce a long-range *R*-curve behavior which would result additionally in an improved thermal-shock damage resistance. The present approach attempts to calculate the stress distribution in duplex ceramics which is the basis for the understanding of fracture processes. Furthermore, the influence of the fabrication conditions on the efficiency of pressure zones in duplex structures is investigated.

2 The Duplex Concept

The structure of duplex ceramics consists of a ceramic matrix A and a spherical pressure zone component B which is homogeneously dispersed within A in the form of spheres (Fig. 1). B contains high amounts of unstabilized ZrO_2 particles. The volume expansion of B due to the spontaneous or stress-induced tetragonal/monoclinic (t/m) transformation of ZrO_2 produces compressive stresses within B and radial compressive and tensile hoop stresses around B.

2.1 Stress distribution

The theory of stresses around inclusions in an isotropic medium is well established. Selsing[14]

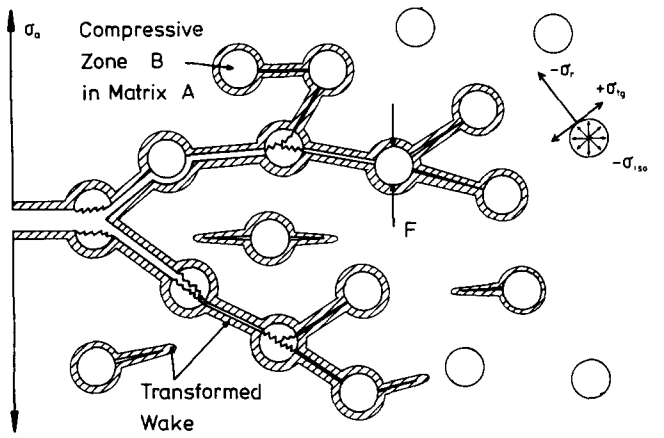

Fig. 1. Schematic crack propagation in a duplex-ceramic with a TZP-matrix.

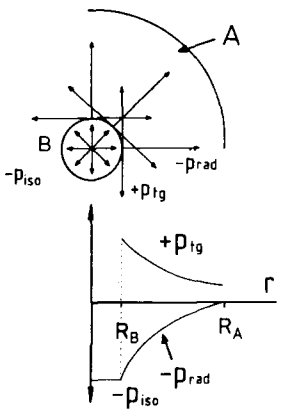

Fig. 2. Basic model of a duplex-structure for the calculation of the stress distribution and the energy approach.

considered the stress distribution in and around a spherical particle embedded in an infinite phase. However, earlier considerations made by Lundin[15] concerning a finite model that considered non-dilute conditions are more realistic. The author defined a system consisting of a spherical particle (here labeled B) with radius R_B embedded in a homogeneous finite spherical system A of radius R_A. It is assumed that the duplex structure is built up of densely packed spheres (74 vol.%) of A, each encasing a spherical B core (Fig. 1). The voids between the A spheres are taken to be stress-free and, hence, will not be considered. The volume fraction, V_f, of B can therefore be related to the volumes of A and B by:

$$V_f = 0{\cdot}74(R_B/R_A)^3 \tag{1}$$

When B is subjected to a volume expansion arising from a volumetric phase change and/or thermal expansion mismatch, the volumetric strain is given by:

$$\varepsilon^v = \Delta V/V + 3(\alpha_A - \alpha_B)\Delta T \tag{2}$$

where $\Delta V/V$ is the volume change of B, α_A and α_B are the expansion coefficients of the components A and B, and ΔT is the temperature difference between fabrication and ambient temperature.

The hydrostatic pressure within the B zones is[15]

$$p^B_{iso} = -c_4(1 - R_B^3/R_A^3) \tag{3}$$

$$c_4 = \frac{c_1}{c_2 + c_3(R_B/R_A)^3} \tag{4}$$

$$c_1 = 2/3E_AE_B\varepsilon^v \tag{5}$$

$$c_2 = 2E_A(1 - 2\mu_B) + E_B(1 + \mu_A) \tag{6}$$

$$c_3 = 2[E_B(1 - 2\mu_A) - E_A(1 - 2\mu_B)] \tag{7}$$

where E_A, E_B, μ_A and μ_B are the Young's moduli and Poisson's ratios of A and B, respectively.

Around B are radial compressive (−) and tangential tensile (+) stresses which decrease with increasing distance r from the center of the zones (Fig. 2). At the interface between A and B the radial stress, p^A_{rad}, has the same value as the hydrostatic pressure, p^B_{iso}, inside B. p^A_{rad} is zero for $r = R_A$, whereas the tangential stresses, p^A_{tg}, reaches a finite value:

$$p^A_{rad}(r) = -c_4(R_B^3/r^3)(1 - r^3/R_A^3) \tag{8}$$

$$p^A_{tg}(r) = 1/2c_4(R_B^3/r^3)(1 + 2r^3/R_A^3) \tag{9}$$

2.2 Stress intensity at the A–B interface

The fracture behaviour of duplex ceramics is severely affected by the residual stress field around B. Cracks will form from small pre-existing defects at or near the inclusion–matrix interface. The frequency of fracture incidence from inclusions increases with increasing number of inclusions—primarily because the probability of locating an inclusion in the tensile area increases.[13] Generally it is found that the incidence of cracking at inclusions increases as the inclusion size increases.[11,13,16] This is due to the simultaneously increasing stress intensity at interfacial defects. An additional size effect can occur if the interfacial defects exhibit a statistically related size distribution. Then the probability that a crack will propagate at a certain stress increases as the interface area is increased.[13] The incidence of crack development is determined by the magnitude of the stress intensity factor, K, at interfacial defects. If K exceeds the critical value, K_c, of the matrix (or inclusion), the cracks will propagate.

Evans[13] has derived an expression for the stress intensity of a crack around an inclusion under internal pressure due to thermal expansion mismatch between inclusion and matrix under an applied stress, thereby using the stress approach of Selsing.[14] Swain[17] observed that a crack first

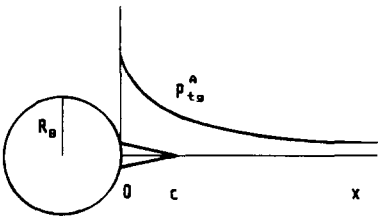

Fig. 3. Coordinate system for the calculation of crack initiation from a matrix–inclusion interfacial defect of length c.

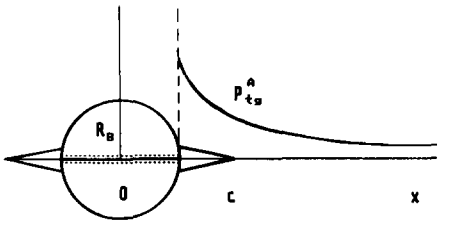

Fig. 4. Coordinate system for the calculation of crack propagation from an annular crack of width c around an inclusion.

initiates at some site about the inclusion before completely encircling it. The author followed an approach adopted from Lawn & Evans[18] for the initiation of cracks beneath a pointed indenter. Lawn & Evans made a simple linear approximation for the stress field up to a certain distance from the initiation site and thereafter set the stress as zero.

In this paper an expression for spontaneous crack initiation and propagation in duplex ceramics is derived on the basis of the Lundin stress model. First crack initiation at any site of B is considered following Swain. The stress intensity for a three-dimensional crack of length c with coordinate system shown in Fig. 3 is[19]

$$K = \frac{2}{(\pi c)^{1/2}} \int_0^c \frac{x p^A_{tg}}{(c^2 - x^2)^{1/2}} \, dx \tag{10}$$

Substituting for p^A_{tg} leads to

$$K = \frac{2}{(\pi c)^{1/2}} \int_0^c \left[0{\cdot}5 c_4 \left(2{\cdot}7 V_f + \frac{R_B^3}{(R_B + x)^3} \right) \right] \times \frac{x \, dx}{(c^2 - x^2)^{1/2}} \tag{11}$$

Since integration of eqn (11) causes difficulties because of the term $R_B^3/(R_B + x)^3$, a simplified Taylor series expansion for $x/R_B < 0{\cdot}2$ is used:

$$\frac{R_B^3}{(R_B + x)^3} \simeq (1 - 3x/R_B) \tag{12}$$

Upon integrating, with $\beta = c/R_B$,

$$K = (R_B \beta/\pi)^{1/2} \{ [(1 + 2{\cdot}7 V_f) - 3\pi\beta/4] c_4 \} \tag{13}$$

For $V_f = 0$ eqn (13) is identical with the expression derived by Swain,[17] who used the Selsing stress approach. An interface-related defect of a critical length β_c will start to propagate when K exceeds the value K_c^A of the matrix. Then eqn (13) can be written in terms of the critical volume expansion, ε_c^v, of the B zones:

$$\varepsilon_c^v \geq 3 \frac{c_2 + 1{\cdot}35 V_f c_3}{2 E_A E_B} \left[\frac{(\pi/\beta R_B)^{1/2} K_c^A}{1 + 2{\cdot}7 V_f - 3\pi\beta/4} \right] \tag{14}$$

From eqn (14) it may readily be seen that a crack initiation from interfacial defects is favored for increasing R_B, V_f, E_A and E_B, as well as for decreasing K_c^A.

Once a crack has initiated for the conditions made in eqn (14) it is assumed that the crack encircles B. Further propagation leads to the model of an annular crack of width c located at the interface of B, as shown in Fig. 4. The stress intensity due to the residual stresses can be estimated for this configuration following an approach derived by Green[20] who, however, used the Selsing stress approach. Inclusion and crack can be considered penny-shaped with radius $(c + R_B)$. The stress acts across the crack surface only for $R_B \leq x \leq (c + R_B)$, where x is the distance from the inclusion center. For this axisymmetric case[21]

$$K = \frac{2}{[\pi(c + R_B)]^{1/2}} \int_{R_B}^{c + R_B} \frac{x p^A_{tg}}{[(c + R_B)^2 - x^2]^{1/2}} \, dx \tag{15}$$

Integration gives

$$K = \left[\frac{\beta R_B (\beta + 2)}{\pi(\beta + 1)} \right]^{1/2} \left[\left(\frac{1}{(\beta + 1)^2} + 2{\cdot}7 V_f \right) c_4 \right] \tag{16}$$

and

$$\varepsilon_c^v \geq 3 \frac{c_2 + 1{\cdot}35 V_f c_3}{2 E_A E_B} \frac{[\pi(\beta + 1)]^{1/2}}{[\beta R_B (\beta + 2)]^{1/2}} \times \frac{K_c^A}{[1/(\beta + 1)^2 + 2{\cdot}7 V_f]} \tag{17}$$

For $V_f = 0$ eqn (16) is identical with the expression derived by Green.[20] The conditions for crack initiation and propagation are only valid if it is assumed that the propagating crack is not dissipating stored energy and is, hence, not affecting the stresses in front of the crack tip. Equation (17) gives a similar dependance of ε_c^v on the important parameters V_f, R_B, E_A and E_B, as in eqn (14). Figure 5 illustrates the dependency of the normalized K as a function of β according to eqn (13) for $0 < \beta < 0{\cdot}2$ and eqn (16) for $\beta > 0{\cdot}1$.

Spontaneous cracking will occur when K exceeds

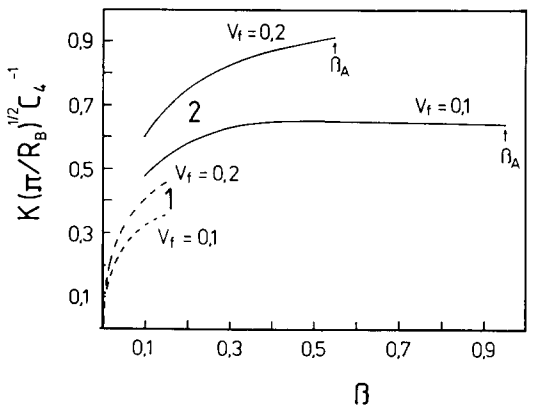

Fig. 5. Plot of β versus $(K/c_4)(\pi/R_B)^{1/2}$ for eqns (13) and (16).

K_c^A for a critical β_c value. If $K > K_c^A$ for β_A $(R_A - R_B)/R_A \geq \beta \geq \beta_c$, the crack will propagate to the end of the A sphere, β_A, linking up with cracks of neighboring A spheres. For duplex ceramics with a B content $V_f \geq 0{\cdot}1$ the steep increase of K with increasing β in Fig. 5 indicates that, once K exceeds the toughness of the matrix for small cracks, the crack will propagate uncontrollably to the end of the A sphere, linking up with cracks in neighboring spheres and causing a crack network through the whole specimen. However, this will only happen if the matrix toughness does not rise upon crack growth, i.e. exhibits no pronounced R-curve behavior.

2.3 Energy approach for crack linking

Previous studies of the energetics of cracking about inclusions with thermal expansion coefficients different from the matrix have been made by Straub,[11] Schueller & Staerk,[22] and Davidge & Green.[12] Davidge & Green used the simplified stress approaches of Selsing[14] and Weyl.[23] Straub followed Schueller & Staerk in deriving an expression for the stored elastic energy based on the Lundin stress model, but neglected the contribution of the Poisson's ratios to the amount of the elastic stored energy.

In this paper the conditions for spontaneous crack linking in duplex ceramics upon cooling are calculated. Since only a neglectable small fraction of the total elastic energy is stored within the voids between the A spheres for $V_f \leq 0{\cdot}2$, the voids are assumed to be energy-free. When a crack links B zones it is supposed to cut the A spheres into ideal halves. Half of the stored energy, U_{el}^{AB}, within the volume $4/3\pi R_A^3$ is expected to be released when the crack creates a new surface area of $2\pi R_A^2$ in one AB-sphere system. Following Prescott,[24] the stored elastic energy, U_{el}, in an element of material subjected to orthogonal tensile (or compressive) stresses p_1, p_2 and p_3 is

$$U_{el} = 1/(2E)[(1+\mu)(p_1^2 + p_2^2 + p_3^2) - \mu(p_1 + p_2 + p_3)] \quad (18)$$

The total stored energy within one B sphere is

$$U_{el}^B = (2/E_B)c_4^2 \pi R_B^3 (1 - 2\mu_B)(1 - 1{\cdot}35V_f)^2 \quad (19)$$

In A the magnitude of the stresses depends on r. Therefore, the total stored energy within one A sphere is obtained by integration:

$$U_{el}^A = 1/(2E_A)\int_{R_A}^{R_B} [(1+\mu_A)(p_{rad}^{A^2} + 2p_{tg}^{A^2}) - \mu_A(p_{rad}^A + 2p_{tg}^A)^2]\,dV \quad (20)$$

Upon integrating

$$U_{el}^A = (2/E_A)c_4^2 \pi R_B^3 (1 - 1{\cdot}35V_f) \times [(0{\cdot}5 + 1{\cdot}35V_f) + \mu_A(0{\cdot}5 - 2{\cdot}7V_f)] \quad (21)$$

The total stored energy within one A sphere (with a B core), U_{el}^{AB}, is the sum of eqns (19) and (21). Assuming a crack propagating radially from an interfacial defect under critical stress intensity conditions, crack linking is assumed to be triggered when

$$1/2U_{el}^{AB} \geq U_S^{AB} \quad (22)$$

with the surface energy

$$U_S^{AB} = 2\pi(R_A^2 - R_B^2)\gamma_A + 2\pi R_B^2 \gamma_B \quad (23)$$

where γ_A and γ_B are the specific surface energies of A and B, respectively. For the condition in eqn (22), combining eqns (1), (19), (21) and (23),

$$\varepsilon_c^v \geq 3\frac{c_2 + 1{\cdot}35V_f c_3}{2E_A E_B R_B^{1/2} c_5^{1/2}} \times \left[\frac{2E_A E_B[(0{\cdot}818/V_f^{2/3} - 1)\gamma_A + \gamma_B]}{(1 - 1{\cdot}35V_f)}\right]^{1/2} \quad (24)$$

with

$$c_5 = (1 - 2\mu_B)(1 - 1{\cdot}35V_f)E_A + [(0{\cdot}5 + 1{\cdot}35V_f) + \mu_A(0{\cdot}5 - 2{\cdot}7V_f)]E_B \quad (25)$$

For $\varepsilon^v \geq \varepsilon_c^v$ enough elastic energy is available to trigger spontaneous crack linking of B zones. Equations (24) and (17) give similar results, although eqn (24) also takes the toughness of B into account. However, for either small values of V_f or of γ_B the influence of B is neglectable. A tough matrix component with low Young's modulus represents a suitable basis for the design of duplex ceramics.

3 Experimental Procedure

The powders for the matrix (component A) were either supplied by Tosoh, Japan (2Y-TZP, 3Y-TZP,

3Y-TZP + 20 wt% Al_2O_3) in an agglomerated state or were prepared by spray drying[25] (Al_2O_3 and m-ZrO_2-toughened Al_2O_3). Different attrition-milled (2h in water) mixtures of Al_2O_3 (CT 8000 SG, Alcoa) and 35, 50, 80 vol.% m-ZrO_2 (Dynazirkon F, Dynamit Nobel), and pure m-ZrO_2 were used as inclusion component B and were also prepared by spray drying.

For further discussions the matrix components A, i.e. 2Y-TZP, 3Y-TZP, 3Y-TZP + 20 wt% Al_2O_3 and Al_2O_3 are labeled 2YZ, 3YZ, 3YZ20A, and AO, respectively. The pressure zone components B, i.e. Al_2O_3 + 35, 50, 80 vol.% m-ZrO_2 and pure m-ZrO_2 are labeled az35, az50, az80 and z100, respectively. For extra small (< 16 μm diameter), small (16–32 μm diameter), intermediate (32–45 μm diameter) and large (45–65 μm diameter) pressure zones the subscripts XS, S, M and L, are used, respectively. The duplex ceramic labeled e.g. 3YZ–20az50$_s$ consists of 20 vol.% of small pressure zones composed of Al_2O_3 + 50 vol.% m-ZrO_2 dispersed within a 3Y-TZP matrix.

Different compositions of A and B, both in the form of spherical agglomerates, were dry tumble mixed for 12 h. The agglomerate mixtures were cold isostatically pressed at 950 MPa. The green compacts were sintered at 1500°C for 2 h and hot isostatically pressed (HIPed) at 200 MPa at 1600°C for 10 min in N_2. Samples were cut into square rods of dimensions 3·5 × 3·5 × 45 mm. The monoclinic-phase fraction of polished and fractured surfaces was determined by the X-ray intensity ratio.[26] The ZrO_2 transformation on fractured surfaces depends on the fracture stress. To achieve uniform fracture stress conditions, especially for ceramics of different strength, the samples were notched by a 30 kg Vickers indentation to achieve a comparable modulus of rupture. The critical volume expansion, ε_c^v, for spontaneous crack initiation and zone linking was calculated using the stress intensity and energy approaches proposed in the previous sections. The analytical data were compared with the experimental results.

4 Results and Discussion

4.1 Compaction

The green density of cold isostatically pressed A/B mixtures varied between 56·5 and 65·0% theoretical density (T.D.). Generally, the green density of the composites coincides nearly with the values which can be calculated from the respective values of the A and B components. With increasing pressure, the generally smaller B agglomerates are deformed within the voids among the larger A agglomerates. The large spheres contain mostly their rounded shape (Fig. 6). The deformability depends on the agglomerate strength which is influenced by the physical properties of the powders and the spray drying conditions.[25]

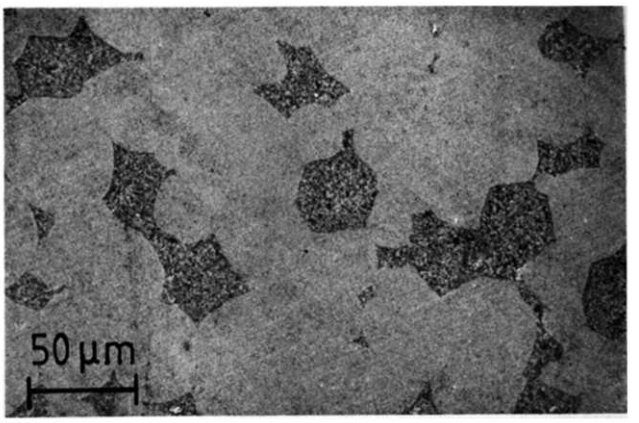

Fig. 6. Slice through a green specimen of 3YZ20A–20az50$_S$. The dark B zones are deformed whereas the matrix agglomerates mostly retain their rounded shape.

4.2 Sintered composites

Duplex ceramics are not sintering uniformly but zonewise. With respect to the sintering behavior of the components A and B two cases will be considered:

(i) Both A and B compositions exhibit a similar sintering behavior. Duplex ceramics consisting of congruently sintering components (e.g. 2YZ, 3YZ, 3YZ20A with az80 or z100 (Fig. 7); AO with az35 or az50) reach high sintering densities.

(ii) The sintering behavior of A and B is different, i.e. A and B are sintering incongruently. The matrix A starts at a lower temperature, sinters at a higher shrinkage rate, and attains a higher density (Fig. 8). Incongruently sintering components are e.g. 2YZ, 3YZ, 3YZ20A and az35 or az50 (Fig. 7).

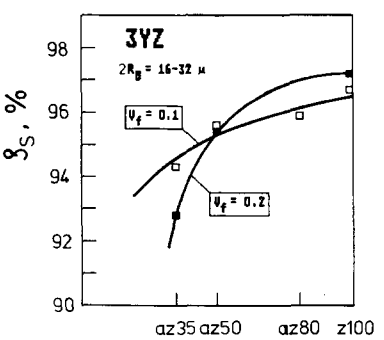

Fig. 7. Sintered density, ρ_S, in % T.D. of 3YZ systems with different B components.

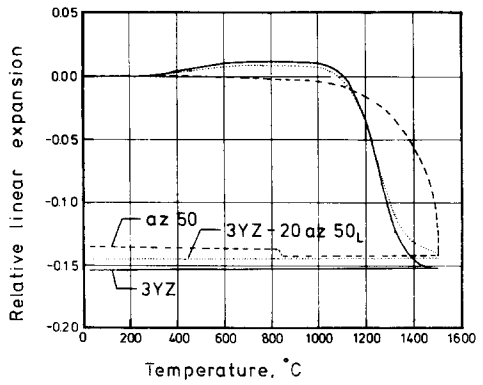

Fig. 8. Sintering density, ρ_s, in % T.D. of 3YZ–20az50$_L$ when compared with the pure components.

Figure 9 shows that the sintering density decreases with increasing volume fraction and size of B. It seems that the B zones are subjected to a compressive strain in the beginning of densification. The still green B material is compressed to a dense particle packing. When the sintering temperature of B is reached the compressive forces may support sintering of B zones. However, this situation is gradually changing at elevated temperatures when the matrix completes sintering. Now a further shrinkage of the B zones is hindered by tensile stresses acting on the A–B interface due to the already densified matrix. The B zones remain porous, made up by large grains (Fig. 10). The sintering density of the resulting duplex composite is low. The influence of time is not yet well understood. Slow heating rates (5–10°C/min) produce denser duplex structures than fast heating (20°C/min) whilst the sintering density of the pure matrix materials is not affected by using different heating rates. Probably a slowly increasing pressure on B zones during sintering is promoting their densification.

4.3 HIPed composites

After HIPing for 10 min in N_2 most duplex ceramics are dense with 99–100% T.D. Structures consisting

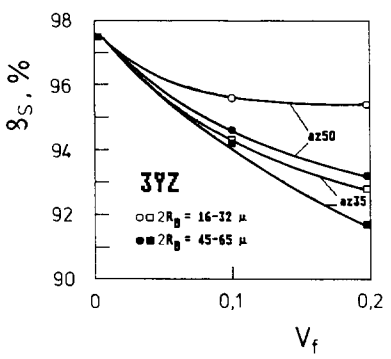

Fig. 9. Sintered density in % T.D. of 3YZ systems as a function of the volume fraction and zone size of az35 and az50.

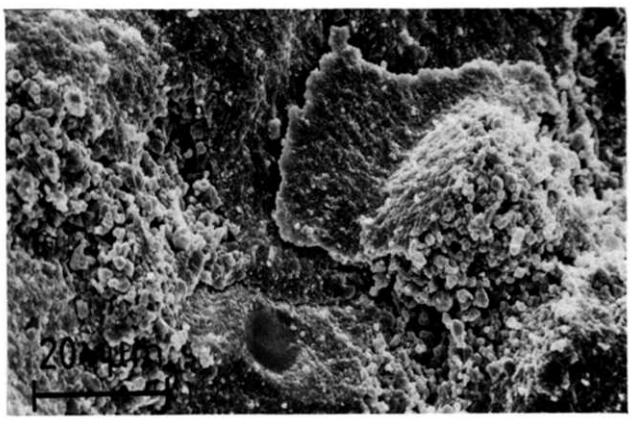

Fig. 10. Fracture surface of 3YZ–20az35$_S$. The B zones are porous and contain large grains.

of incongruently sintering components reach 98% T.D. The B zones are so highly compressed that they cannot be easily distinguished from the matrix, except by their coarser grains.

4.4 Transformability of B-ZrO_2

The spontaneous transformation of ZrO_2 particles in B zones dispersed within TZP and TZP-containing matrix materials is not complete after sintering. After HIPing the monoclinic fraction is further reduced, but can be increased to a limited degree by choosing other HIPing conditions.[27] The transformation completes during fracture in both sintered and HIPed materials. A part of the t-ZrO_2 is thought to be stabilized by the hydrostatic pressure in B which develops on cooling due to a positive thermal expansion mismatch ($\alpha_A > \alpha_B$) between A and B and the beginning transformation. This presupposes highly densified B zones. In 2YZ–az35 systems the transformation is totally suppressed after HIPing. The relatively larger increase of the m/(t + m) ratio on the fractured duplex surface when compared to the respective data of the matrix is both due to the complete transformation in B and additional stress induced transformation of A material around the B zones.

4.5 Predictions and observations of spontaneous cracking

Spontaneous cracking around inclusions could be observed on polished surfaces of 3YZ and 3YZ20A with 20z100$_S$ and AO–20az35$_S$ and AO–10az50$_S$. The cracks never end isolated in the matrix but always link up with neighboring pressure zones, developing a crack network over the whole specimen surface. No cracking occurs in 3YZ and 3YZ20A with up to 20 vol.% of large zones of az35 and az50, with up to 20 vol.% of az80$_S$, 10 vol.% of az80$_L$, and

10 vol.% of $z100_S$, and in AO with up to 10 vol.% of $az35_S$.

Using eqns (14), (17) and (24), the critical volume expansion, ε_c^v, for spontaneous cracking can be calculated under the following conditions:

(i) K_c^A for the matrix is taken to be 3 $MPam^{1/2}$ according to the starting value of the K^R curve of 3YZ20A.[28] The K^R curve of AO is not known but expected to be as flat as the K^R curve of 3YZ20A.[28] AO and 3YZ20A exhibit the same K_{Ic}. For this reason the same K_c^A value is assumed for both AO and 3YZ20A.

(ii) It is assumed that cracking starts from an interfacial defect with a length of 3 μm which is about the average grain size of the zones. It is expected that the crack encircles the B zone completely when a radial extension of 5 μm is achieved. This is presumed to be the initial length of the annular crack from which the crack further extends radially.

(iii) Since the first cracks will form at the largest zones, the upper limits instead of the average values of the zone size distributions, i.e. $2R_A = 32$ and 65 μm for small and large zones, are considered.

(iv) The Young's moduli, E_A and E_B, are estimated by comparing the values of the duplex composites with the respective data of the pure matrix components.[28] E_A of 3YZ20A is 247 GPa. This leads to the values of *c.* 250, 250, 210 and 190 GPa for az35, az50, az80 and z100, respectively. E_A of AO is 360 GPa. In AO–az35 systems E_B of az35 is then *c.* 300 GPa.

(v) The specific surface energy of 3YZ20A and AO can be estimated using K_{Ic} and E_A^{28}. γ_A is 35 and 24 J/m^2, respectively. The γ_B values for the B components az35, az50, az80 and z100 are taken to be 12, 9, 5 and 0 J/m^2, respectively.

vi) The Poisson's constants, μ, and thermal expansion coefficients, α, are taken from the literature: μ of 3YZ20A, AO, az35, az50, az80 and z100, is 0·26, 0·23, 0·24, 0·25, 0·26 and 0·27, respectively; α is taken to be 9·9, 8·0, 7·9, 7·8, 7·6 and 7·5 × 10^{-6}, respectively.

The ε_c^v curves resulting from eqns (14), (17) and (24) are shown in Figs 11, 12 and 13, respectively, for small and large zones as a function of V_f. For comparison, the maximum expansion, ε_{max}^v, for the B zone compositions, az35, az50, az80 and z100, are calculated presupposing that the ZrO_2 transformation is complete and causes a 4% volume expansion. The thermal expansion mismatch between A and B has been taken into consideration in this calculation. ε_{max}^v is shown as broken horizontal lines. If ε_{max}^v exceeds ε_c^v for the respective composition, cracking is expected.

As can be seen from Figs 11 to 13 the ε_c^v curves decrease with increasing V_f, R_B, E_A and E_B. Equation (14) predicts no spontaneous crack initiation for 3YZ20A with az35 and az50. For more than 12 vol.% of $az80_L$, 15 vol.% of $z100_S$ and 5 vol.% of $z100_L$, however, eqn (14) predicts crack intiation at

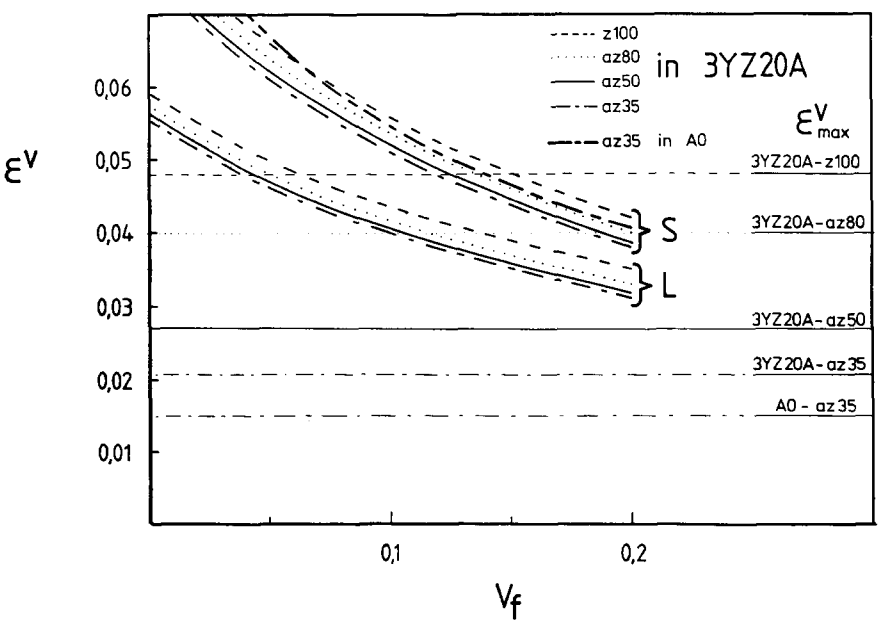

Fig. 11. Plot of eqn (14) in the form of ε^v versus V_f. When the maximum volume expansion of the pressure zones of a certain composition, ε_{max}^v, shown as horizontal lines, exceeds the respective ε_c^v-curves, spontaneous crack initiation is expected.

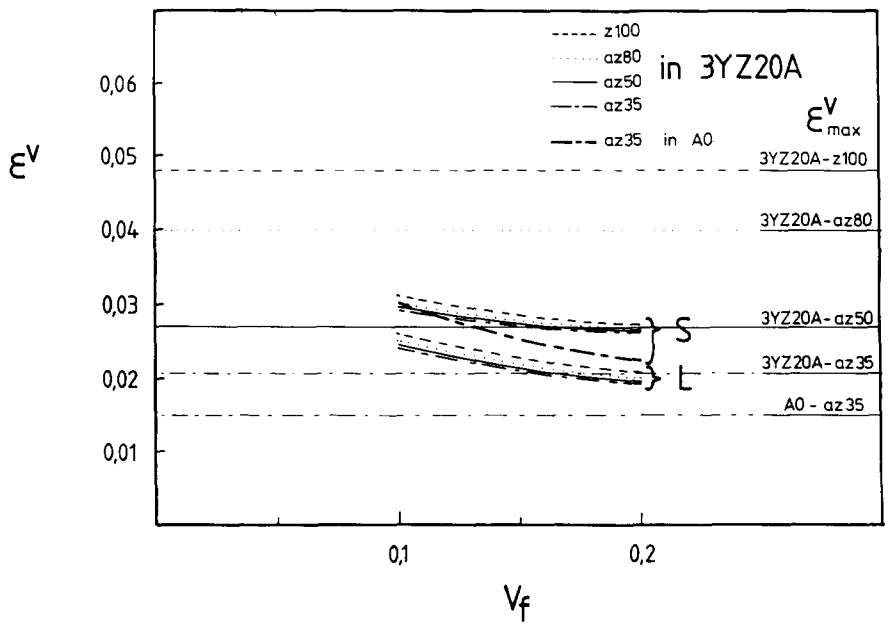

Fig. 12. Plot of eqn (17) in the form of ε^v versus V_f. When the maximum volume expansion of the pressure zones of a certain composition, ε^v_{max}, shown as horizontal lines, exceeds the respective ε^v_c-curves, spontaneous crack propagation is expected.

the presssure zone/matrix interface. This is in good agreement with the observations. The matrix AO is more sensitive with respect to spontaneous cracking than TZP or TZP-containing matrices because of its high Young's modulus. No cracking should occur with small B zones of az35. The fact that cracks develop nevertheless during cooling is probably due to an underestimation of the initial defect length.

Equations (17) and (24) give similar results. Once a crack has initiated it should extend immediately to neighboring zones, developing a crack network. As predicted by eqns (17) and (24), B zones with 50 vol.% ZrO_2 or more should cause crack propagation and the development of a crack network in 3YZ20A, supposing that a crack could initiate and encircle the zone. The assumption that a crack network would form once a crack has initiated is in good agreement with the observations. In contrast to this is the behavior of AO systems. Although no crack initiation should occur according to eqn (14), the development of a crack network is observed, as predicted by eqn (17).

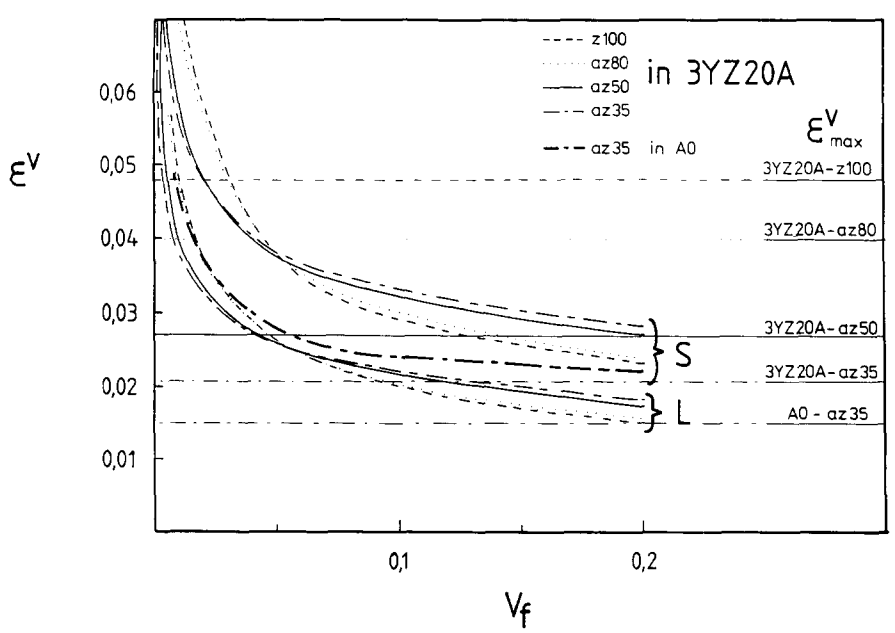

Fig. 13. Plot of eqn (24) in the form of ε^v versus V_f. When the maximum volume expansion of the pressure zones of a certain composition, ε^v_{max}, shown as horizontal lines, exceeds the respective ε^v_c-curves, spontaneous crack propagation is expected.

The effect of the incorporation of pressure zones on the strength and toughness of these composite materials will be discussed in a complementary paper.

5 Conclusion

The stress distribution within duplex structures has been calculated on the basis of the Lundin stress approach. The stress intensity factor for a small radial defect located at the interface between the pressure zone and its environmental matrix can be calculated as a function of volume expansion, amount and size of the zones. By comparing the stress intensity factor with the matrix toughness, the conditions for crack initiation from such zone–matrix interfacial defects can be estimated. It is assumed that the crack first encircles the pressure zone before further radial extension. The condition for the further crack propagation can then be estimated using a similar stress-intensity approach for an annular crack around the zone. The stress-intensity calculation method gives similar conditions when compared with energy considerations. The predictions for crack initiation and propagation are in reasonable agreement with observations. The fabrication of duplex ceramics presupposes the knowledge of the sintering behavior of their components. Incongruent sintering behavior of the components leads to highly porous pressure zones. The transformability of ZrO_2 particles within the zones depends on the density of the zones after fabrication and the thermal mismatch strain between matrix and zones. It is nearly completely reduced in zones which are dispersed in HIPed TZP or TZP-containing matrix materials.

Acknowledgement

Supported by the Stiftung Volkswagenwerk under contract number I/61 901 and I/64 239. The authors thank Mike Swain for valuable suggestions and for the correction of this paper.

References

1. Evans, A. G., The new generation of high toughness ceramics. In *Ceramic Microstructures*, ed. J. A. Pask & A. G. Evans. Plenum Press, New York, 1987, p. 775.
2. Evans, A. G. & McMeeking, R. M., On the toughening of ceramics by strong reinforcements. *Acta Met.*, **34** (1986) 2435–47.
3. Claussen, N., Strengthening strategies for ZrO_2-toughened ceramics at high temperatures. *Mat. Sci. Eng.*, **71** (1985) 23–7.
4. Nettleship, I. & Stevens, R., Tetragonal zirconia polycrystals (TZP)—a review. *Int. J. High Tech. Ceram.*, **3** (1987) 1.
5. Hasselman, D. P. H., Unified theory of thermal shock fracture initiation and crack propagation of Brittle ceramics. *J. Am. Ceram. Soc.*, **52** (1969) 600–4.
6. Larson, D. R., Coppola, J. A., Hasselman, D. P. H. & Bradt, R. C., Fracture toughness and spalling behavior of high-alumina refractories. *J. Am. Ceram. Soc.*, **10** (1974) 417–21.
7. Swain, M. V., R-Curve behavior of magnesia partially stabilized zirconia and it's significance to thermal shock. *Fract. Mech. Ceram.*, **6** (1983) 355–70.
8. Claussen, N. & Petzow, G., German Patent DE 3233019, 1982; US Patent 4, 506 024, 1983, Japanese Patent, 64567/84.
9. Claussen, N., Umwandlungsverstaerkte keramische Werkstoffe. *Z. Werkstofftechnik*, **13** (1982) 138–95.
10. Claussen, N. & Lutz, E., Microstructural design of oxide ceramic composites for high-thermal shock resistance. In *Proc. of the Int. Symp. of Fine Ceramics*, Arita, Japan, 1987.
11. Straub, F., Ueberlegungen zur Festigkeit keramischer Werkstoffe. *Ber. DKG*, **46** (1969) 299–308.
12. Davidge, R. W. & Green, T. J., The strength of two-phase ceramic glass materials. *J. Mat. Sci.*, **3** (1968) 629–34.
13. Evans, A. G., The role of inclusions in the fracture of ceramic materials. *J. Mat. Sci.* **9** (1974) 1145–52.
14. Selsing, J., Internal stresses in ceramics. *J. Am. Ceram. Soc.*, **44** (1961) 419.
15. Lundin, S. T., In *Studies on Triaxial Whiteware Bodies*, ed Almquist & Wiksell. Royal Institute of Technology, Stockholm, Sweden, 1959.
16. Lange, F. F., Fracture mechanics and microstructural design. *Fract. Mech. Ceram.*, **4** (1978) 799–838.
17. Swain, M. V., A fracture mechanics description of the microcracking about NiS inclusions in glass. *J. Non-Cryst. Solids*, **38–39** (1980) 451–6.
18. Lawn, B. R. & Evans, A. G., A model for crack initiation in elastic/plastic indentation fields. *J. Mat. Sci.*, **12** (1977) 2195–208.
19. Sih, G. C., *Handbook of Stress Intensity Factors*. Lehigh University Press, Lehigh, 1973.
20. Green, D. J., Stress-induced microcracking at second-phase inclusions. *J. Am. Ceram. Soc.*, **64** (1981) 138–41.
21. Barenblatt, G. I., In *Advances in Applied Mechanics, No. 7*, ed. H. L. Dryden, Th. von Karman & G. Kuerti. Academic Press, New York, 1962, pp. 55–126.
22. Schueller, K. H. & Staerk, K., Zur Theorie der Gefuegespannungen im Porzellan. *Ber. DKG*, **44** (1967) 458–62.
23. Weyl, D., Ueber den Einfluss innerer Spannungen auf das Gefuege und die mechanische Festigkeit des Porzellans (Influence of Internal Strains on Texture and Mechanical Strength of Porcelains). *Ber. DKG*, **36** (1959) 319–24.
24. Prescott, J., In *Applied Elasticity*. Longmans, 1924, p. 188.
25. Kumar, D., Ladisch, R., Lutz, E. & Claussen, N., Pulveraufbereitung mit dem Spruehtrockner. *Ber. DKG*, **65** (1988) 161.
26. Garvie, R., Stabilisation of the tetragonal structure in zirconia microcrystals. *J. Phys. Chem.*, **82** (1978) 218–24.
27. Lutz, E. & Claussen, N., Toughening of oxide ceramics by residual stress domains. In *Proc. 3rd Int. Symp. on Ceramic Mat. & Comp. for Eng.*, Vol. 3, ed. V. J. Tennery. The American Ceramic Society, Westerville, OH, 1989, pp. 1020–30.
28. Lutz, H. E., Aufbau und Eigenschaften von Al_2O_3- und ZrO_2-Keramiken mit kugeligen Druckzonen. PhD Thesis, Technical University of Hamburg–Harburg, FRG, 1989.